Preprints of the 21st IFAC World Congress (Virtual)
Berlin, Germany, July 12-17, 2020

Development and Design Optimization of 2Y Hexarotor with Robustness against Rotor Failure ⋆

Shunsuke Mochida * **Remma Matsuda** ** **Tatsuya Ibuki** *
Mitsuji Sampei *

* *Tokyo Institute of Technology, Tokyo, Japan*
(e-mail: mochida@sl.sc.e.titech.ac.jp,
{ibuki, sampei}@sc.e.titech.ac.jp).
** *Panasonic Mobile Communications,*
(e-mail: matsuda@sl.sc.e.titech.ac.jp)

Abstract: This paper presents a novel hexarotor unmanned aerial vehicle (UAV) with robustness against an arbitrary rotor-failure, called full robustness, and a design method to maximize its manipulability while ensuring the full robustness. First, the dynamical model of a hexarotor UAV and the novel structure with 2Y shape and twisted angles are presented. A hexarotor with this structure is named as 2Y hexarotor. The 2Y hexarotor has higher flight efficiency than other existing hexarotor structures with full robustness. Second, the full robustness of the 2Y hexarotor is proved, and a quantitative measure to evaluate the full robustness is introduced. Then, the quantitative measure for the full robustness is used to calculate the optimal twisted angles. Finally, the dynamic manipulability measure (DMM) is introduced to evaluate the maneuverability. A design method is defined as the maximization of the DMM under constraints regarding the quantitative measure for the full robustness and the condition to avoid overlapping rotors. The design method is applied to the 2Y hexarotor with the optimal twisted angles.

Keywords: Aerospace control, Autonomous mobile robots, Design optimization, Stability robustness, System failure and recovery, Unmanned aerial vehicles

1. INTRODUCTION

Task automation with a multirotor unmanned aerial vehicle (UAV) is one of the hot topics in robotics. It has been studied actively to automate tasks such as building inspection (Vazquez-Nicolas et al. (2018)), load transportation (Liang et al. (2017)), and work with a robotic arm (Kim et al. (2013)). A multirotor UAV can move to an arbitrary position in the air with at least four rotors, and thus a quadrotor UAV is one of the typical structures (Bouabdallah et al. (2004); Tayebi and McGilvray (2006)). Furthermore, a hexarotor UAV is also a common structure with redundancy (Kirsch et al. (2016)). The standard quadrotor and hexarotor are shown in Fig. 1. In the standard structure, each rotor is upward oriented and placed on a vertex of the regular polygon so that its rotational direction is opposite to that of adjacent rotors.

A multirotor UAV is required to have the ability to achieve static hovering, called hoverability in this paper, to perform its task. Moreover, we focus on the property that maintains the hoverability even after an arbitrary rotor is failed. This property is called full robustness and required for safe work in a field. A hexarotor UAV is expected to be robust against a rotor failure because of its redundancy. However, it is revealed that the standard hexarotor loses the hoverability after any one rotor is failed in some studies (Giribet et al. (2016); Michieletto et al. (2018); Schneider et al. (2012); Vey and Lunze (2015)). The standard hexarotor with one failed rotor is uncontrollable because it cannot output the roll, pitch, and yaw moments independently. Kamel et al. (2015) proposed fault tolerant control for the standard hexarotor. It is a control scheme that makes the standard hexarotor stay in the air by sacrificing the control of the yaw angle. Then, the vehicle flies while rotating around the yaw axis. This motion might be inappropriate for some tasks because it might damage equipment on the vehicle or surroundings.

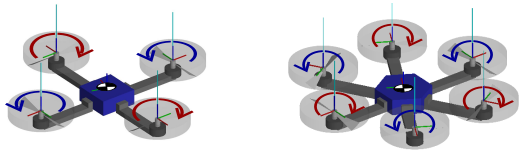

(a) Standard quadrotor (b) Standard hexarotor

Fig. 1. Standard structure of multirotor UAVs: All the rotors are placed on the same plane and in the same direction. Their rotational directions are alternative.

Some researchers proposed the hexarotor structures with robustness against a rotor-failure. Schneider et al. (2012) and Vey and Lunze (2015) showed that the hexarotor UAV with rotational directions of some rotors inverted from the standard hexarotor is robust against a failure of certain rotors. It is a simple structure and achieves the static

⋆ This work has been supported by JSPS KAKENHI Grant Number 16H04383.

hovering even after the certain rotor is failed. However, it is not fully robust, and thus it becomes uncontrollable after another rotor is failed. Giribet et al. (2016) and Michieletto et al. (2018) presented that a hexarotor UAV with all rotors tilted to outside or inside of the vehicle is fully robust. Michieletto et al. (2018) also proposed a fully robust structure that is developed by rotating the position of some rotors around the yaw axis from the standard hexarotor, e.g., Y-shaped hexarotor with three pairs of overlapped two rotors. However, a hexarotor UAV with tilted rotors causes lower flight efficiency than that with all the rotor oriented in the same direction because each rotor generates the thrust force in different directions. On the other hand, in Y-shaped hexarotor, the overlapped rotors degrade the thrust force of the lower rotor (Otsuka and Nagatani (2016)).

This paper presents a novel hexarotor UAV with full robustness. Furthermore, it keeps the flight efficiency by placing each rotor in the same direction and without any overlap. This hexarotor UAV is named as *2Y hexarotor*. The full robustness of the 2Y hexarotor is presented from hoverability analysis with the Equilibrium existence region (EER) proposed in our previous work (Matsuda et al. (2018)). Furthermore, we propose a design scheme of its physical parameters. Two quantitative measures are introduced to design the parameters. One is the dynamic manipulability measure (DMM) to evaluate the manipulability (Yoshikawa (1985)), and the other is the distance between the center of mass (CoM) and the boundary of the EER, called hoverability margin, to evaluate the robustness of the hoverablity. The DMM was introduced for evaluation of manipulator performance in Yoshikawa (1985) at first. In recent studies, Tadokoro et al. (2017) and Anzai et al. (2018) applied the DMM to structure optimization for a fully actuated multirotor UAV. In this paper, we apply it to structure optimization for an underactuated hexarotor UAV. We optimize the parameters to maximize the DMM under the constraint that the hoverability margin is larger than a specific value even after a rotor-failure. This optimization finds the UAV structure with both high manipulability and sufficient robustness against a rotor-failure to perform the task safely.

2. 2Y HEXAROTOR MODEL

In this paper, we ignore the aerodynamic disturbance and dynamics of each rotor. The main symbols used in this paper are listed in Table 1, and $O_{k\times l} \in \mathbb{R}^{k\times l}$ and $I_k \in \mathbb{R}^{k\times k}$ indicate the $k\times l$ zero matrix and $k\times k$ identity matrix, respectively.

2.1 Dynamical Model

We first consider a hexarotor UAV model with a planar structure. Figure 2 shows the dynamical model in the case of the 2Y hexarotor.

Each rotor is oriented in the positive z-axis in Σ_c. Then, the i-th rotor, located at $p_{cr_i} = [x_i, y_i, 0]^T$ in Σ_c, generates the rotor thrust force $f_i \geq 0$ in the rotational axis direction and the counter torque $\kappa_i f_i$ around its rotational axis. The sign of κ_i depends on the rotational direction of the i-th rotor. The rotational direction of each rotor plays an important role in our hoverability analysis. Therefore, we call a rotor which rotates in the clockwise direction *P rotor*, and that which rotates in the counterclockwise direction *N rotor* in this paper. The counter torque constant of the P rotor is positive ($\kappa_i > 0$), and the counter torque of the P rotor is generated in the counterclockwise direction. On the other hand, the counter torque constant of the N rotor is negative ($\kappa_i < 0$), and the counter torque is generated in the clockwise direction.

Table 1. Nomenclature

Symbol	Definition
Coordinate frames	
Σ_o	Inertial frame
Σ_c	Body frame (origin at center of mass)
Vehicle	
$p_{oc} \in \mathbb{R}^3$	Position of center of mass (in Σ_o)
$R_{oc} \in SO(3)$	Attitude (in Σ_o)
$F_c \in \mathbb{R}^6$	Applied wrench (in Σ_c)
$m \in \mathbb{R}$	Mass
$J \in \mathbb{R}^{3\times 3}$	Inertia tensor (in Σ_c)
$\omega \in \mathbb{R}^3$	Body angular velocity (in Σ_c)
$v \in \mathbb{R}^3$	Body translational velocity (in Σ_c)
Rotor	
$i \in \{1, \dots, 6\}$	Index
$p_{cr_i} \in \mathbb{R}^3$	Position (in Σ_c)
$f_i \in \mathbb{R}$	Thrust force
$\kappa_i \in \mathbb{R}$	Counter torque constant

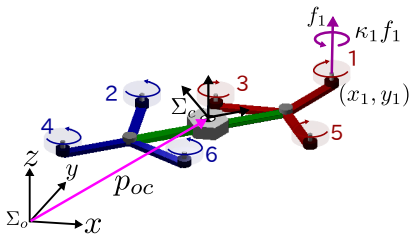

Fig. 2. Dynamical model of 2Y hexarotor: The rotors colored red indicate P rotors, and those colored blue indicate N rotors.

The total wrench of the six rotors applied at the CoM is

$$F_c = \begin{bmatrix} & O_{2\times 6} & \\ 1 & \cdots & 1 \\ y_1 & \cdots & y_6 \\ -x_1 & \cdots & -x_6 \\ \kappa_1 & \cdots & \kappa_6 \end{bmatrix} \begin{bmatrix} f_1 \\ \vdots \\ f_6 \end{bmatrix} =: \begin{bmatrix} & O_{2\times 6} & \\ 1 & \cdots & 1 \\ & C_\tau & \end{bmatrix} u,$$

where $u = [f_1 \ \cdots \ f_6]^T \in \mathbb{R}^6$ and $C_\tau \in \mathbb{R}^{3\times 6}$ is a matrix which maps the rotor thrust forces to the moments of the vehicle. Therefore, the Newton-Euler equation of motion in Σ_c is described by

$$\begin{bmatrix} mI_3 & O_{3\times 3} \\ O_{3\times 3} & J \end{bmatrix} \begin{bmatrix} \dot{v} \\ \dot{\omega} \end{bmatrix} + \begin{bmatrix} \omega \times mv \\ \omega \times J\omega \end{bmatrix} = F_c + \begin{bmatrix} -mgR_{oc}^\top e_3 \\ O_{3\times 1} \end{bmatrix}, \quad (1)$$

where $g > 0$ is the gravity acceleration and $e_3 := [0\ 0\ 1]^T \in \mathbb{R}^3$. Note that a structure of a hexarotor UAV affects only C_τ in (1).

2.2 State Equation

First, we represent R_{oc} by the ZYX Euler angles with the roll, pitch, and yaw angles $r_{oc} := [\phi\ \theta\ \psi]^T \in \mathbb{R}^3$ as follows:

$$R_{oc} = R_z(\psi) R_y(\theta) R_x(\phi). \quad (2)$$

Here $R_x(\cdot), R_y(\cdot), R_z(\cdot) \in SO(3)$ indicate the rotation matrices around x, y, z-axes, respectively.

From (1) and (2), the nonlinear state equation of the hexarotor UAV in Σ_o is described by

$$\dot{\xi} = f(\xi, u), \tag{3}$$

where $\xi := [p_{oc}^T \ \dot{p}_{oc}^T \ r_{oc}^T \ \dot{r}_{oc}^T]^T \in \mathbb{R}^{12}$ is the state vector. The system (3) has a steady-state input u_{ss} that can maintain equilibrium at a state ξ_{ss}. In our hoverability analysis, we consider the linearized system of (3) around (ξ_{ss}, u_{ss}). We can rewrite (3) as $\dot{\xi}_\delta = f_\delta(\xi_\delta, u_\delta)$ with $\xi_\delta := \xi - \xi_{ss} \in \mathbb{R}^{12}$ and $u_\delta := u - u_{ss} \in \mathbb{R}^6$. Then, the linearized system is described by

$$\dot{\xi}_\delta = A\xi_\delta + Bu_\delta \tag{4}$$

with

$$A := \frac{\partial f_\delta}{\partial \xi_\delta}(0,0), \quad B := \frac{\partial f_\delta}{\partial u_\delta}(0,0).$$

All the rotors of a hexarotor UAV with a planar structure are oriented in the upward direction. Therefore, the vehicle orientation at the equilibrium point ξ_{ss} is only the positive direction of the z-axis in Σ_o.

2.3 Structure of 2Y Hexarotor

A structure of a hexarotor UAV is represented by specifying elements of C_τ. We first introduce the structure of the Yaw-Twisted hexarotor based on Michieletto et al. (2018).

Definition 1. Yaw-Twisted hexarotor is a hexarotor UAV whose structure is described by

$$\begin{cases} x_i &= r\cos\left(\frac{i-1}{3}\pi + \alpha\right) \\ y_i &= r\sin\left(\frac{i-1}{3}\pi + \alpha\right) \\ \kappa_i &= \kappa \end{cases} \quad i \in \{1,3,5\},$$

$$\begin{cases} x_i &= r\cos\left(\frac{i-1}{3}\pi + \beta\right) \\ y_i &= r\sin\left(\frac{i-1}{3}\pi + \beta\right) \\ \kappa_i &= -\kappa \end{cases} \quad i \in \{2,4,6\},$$

where $r > 0$ is the length of each rotor arm and $\alpha, \beta \in (-\pi/3, \pi/3]$ are the twisted angles.

Figure 3(a) shows the Yaw-Twisted hexarotor. The Yaw-Twisted hexarotor is obtained by rotating all the P rotors by α and all the N rotors by β around the yaw axis from the standard hexarotor. The Yaw-Twisted hexarotor with $|\alpha - \beta| = \pi/3$ is called Y-shaped hexarotor.

The structure of 2Y Hexarotor is newly presented as follows:

Definition 2. 2Y hexarotor is a hexarotor UAV whose structure is described by

$$\begin{cases} x_i &= l + r\cos\left(\frac{i-1}{3}\pi + \alpha\right) \\ y_i &= r\sin\left(\frac{i-1}{3}\pi + \alpha\right) \\ \kappa_i &= \kappa \end{cases} \quad i \in \{1,3,5\}, \tag{5}$$

$$\begin{cases} x_i &= -l + r\cos\left(\frac{i-1}{3}\pi + \beta\right) \\ y_i &= r\sin\left(\frac{i-1}{3}\pi + \beta\right) \\ \kappa_i &= -\kappa \end{cases} \quad i \in \{2,4,6\},$$

where $l > 0$ is the length between the center of P (N) rotors and the CoM.

Figure 3(b) illustrates the 2Y hexarotor. This structure is developed by respectively translating all the P rotors and all the N rotors by l and $-l$ along the x-axis of Σ_c from the Yaw-Twisted hexarotor. The Yaw-Twisted hexarotor, especially Y-shaped hexarotor, is prone to have an overlap of two rotors. Thus, adding the translation, we obtain the structure without any overlap.

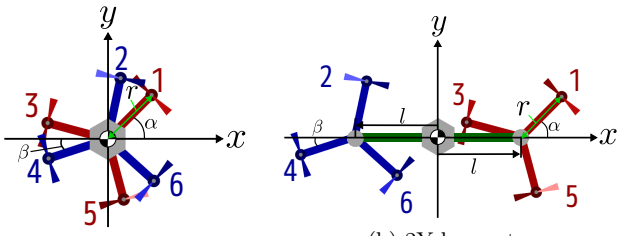

(a) Yaw-Twisted hexarotor (b) 2Y hexarotor

Fig. 3. Structures with twisted angles: (a) The Yaw-Twisted hexarotor is a structure with the twisted angles α, β. (b) The 2Y hexarotor is obtained by adding the translation of rotors to the Yaw-Twisted hexarotor.

3. ROTOR-FAILURE ROBUSTNESS ANALYSIS

This section shows that the 2Y hexarotor is fully robust against a rotor-failure, and gives optimal twisted angles in the sense of the full robustness.

3.1 Geometric Hoverability Analysis Method

We briefly review the hoverability analysis with the EER proposed in our previous work (Matsuda et al. (2018)). First, we consider the condition for a hexarotor UAV to achieve static hovering. We need to analyze the controllability of the UAV system with input constraint $f_i \geq 0$. Matsuda et al. (2018) introduced the matrix B_p by removing the columns which correspond to zero elements in u_{ss} from B, and defined (A, B_p) controllability as follows:

Definition 3. ((A, B_p) controllability). The linearized system (4) is said to be (A, B_p) controllable if the following equation holds for $A \in \mathbb{R}^{12\times12}$, $B_p \in \mathbb{R}^{12\times(n-q)}$. ($q$ is the number of zeros in u_{ss})

$$\mathrm{rank}[B_p \ AB_p \ A^2B_p \ \cdots \ A^{11}B_p] = 12. \tag{6}$$

If the linearized system (3) is (A, B_p) controllable, the original system (3) can be locally stabilized by linear state feedback. We now provide the definition of the hoverability.

Definition 4. (Hoverability (Matsuda et al. (2018))). A hexarotor UAV is said to be *hoverable* if the following two conditions are satisfied:

(i) The original system (3) has at least one equilibrium such that each element of u_{ss} is greater than or equal to zero.
(ii) The linearized system (4) around the equilibrium is (A, B_p) controllable.

Hoverable multirotor UAVs can control their attitude and position without killing the yaw control. The condition (i) can be analyzed using the geometric method as follows:

Fact 5. (Matsuda et al. (2018)). A hexarotor UAV with $|\kappa_i| = \kappa > 0$ for all $i \in \{1, \ldots, 6\}$ has equilibria if and only if the CoM exists in the convex hull composed of the midpoints between an arbitrary P rotor and N rotor on (x, y)-plane in Σ_c.

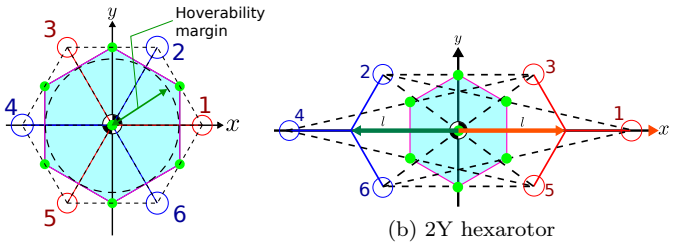

(a) Standard hexarotor (b) 2Y hexarotor

Fig. 4. EER of hexarotor UAV: The green dots indicate the midpoints between each P rotor and N rotor, and the cyan regions indicate the EERs.

Fact 5 enables us to analyze the existence of equilibria with the simple geometric way. The convex hull in Fact 5 is called *Equilibrium existence region (EER)*. The cyan area of Figure 4(a) shows the EER of the standard hexarotor. Note that u_{ss} such that each element is greater than zero exists if the CoM is included in the interior of the EER by properties of linear transformation between two convex sets (Schneider et al. (2012)). From Fact 5, we find the following property about the EER:

Lemma 6. The EER of a hexarotor UAV is invariant under the pair of the translation of all the P rotors by $[x\ y\ 0]^T$ and that of all the N rotors by $[-x\ -y\ 0]^T$ in Σ_c.

Proof. It is trivial because EER is composed of the midpoints between an arbitrary P rotor and N rotor.

Figure 4(b) indicates the EER of the 2Y hexarotor which is obtained by adding the translation of all the P rotors by $[l, 0, 0]^T$ and that of all the N rotors by $[-l, 0, 0]^T$ from the standard hexarotor in Figure 4(a). The EER of the 2Y hexarotor is the same as that of the standard hexarotor. Lemma 6 is used to prove the full robustness of the 2Y hexarotor in the next section.

A multirotor UAV is required to be able to keep the static hovering even after any one rotor is failed. We next introduce the definitions to investigate the full robustness, which are initially defined in Michieletto et al. (2018).

Definition 7. (Rotor-failure (Michieletto et al. (2018))). The i-th rotor is *failed* if it cannot generate any force, i.e., $f_i \equiv 0$.

Definition 8. (Full robustness (Michieletto et al. (2018))). A hexarotor UAV is said to be *fully robust* if it is still hoverable after the i-th rotor is failed for all $i \in \{1, \dots, 6\}$.

The full robustness of a hexarotor UAV can be examined by analyzing the hoverability of each structure obtained by removing an arbitrary rotor from the hexarotor UAV.

Finally, we provide a quantitative measure for the hoverability. This quantitative measure can be used to design an optimal structure for the hoverablity or the full robustness.

Definition 9. For a hoverable hexarotor UAV, the shortest distance between the CoM and the boundary of the EER is called *hoverability margin*.

A hoverable hexarotor UAV is still hoverable if the perturbation of the CoM position is within the hoverability margin. This implies that a hexarotor UAV with a larger hoverability margin can perform its task more safely. The minimum hoverability margin among all the hoverability

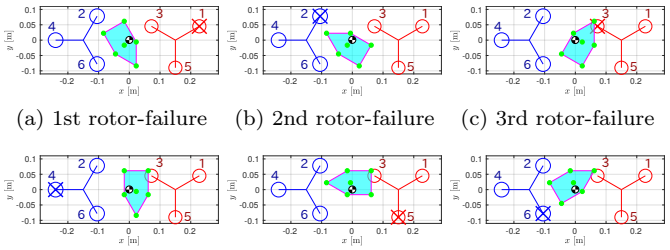

(a) 1st rotor-failure (b) 2nd rotor-failure (c) 3rd rotor-failure

(d) 4th rotor-failure (e) 5th rotor-failure (f) 6th rotor-failure

Fig. 5. Full robustness of 2Y hexarotor: The structure with $(r, l, \alpha, \beta) = (0.09\ \text{m}, 0.15\ \text{m}, \pi/6, 0)$ is still hoverable even after any one rotor is failed.

margin of a hexarotor UAV with an arbitrary rotor-failure can be used to evaluate the full robustness.

For analysis examples of the geometric hoverability method, refer to Matsuda et al. (2018).

3.2 Rotor-Failure Robustness of 2Y Hexarotor

We introduce the following fact about the Yaw-Twisted hexarotor proved in Michieletto et al. (2018).

Fact 10. The Yaw-Twisted hexarotor with $|\alpha - \beta| \in (0, \pi/3]$ is fully robust.

Fact 10 is also confirmed by checking whether the Yaw-Twisted hexarotor with the i-th rotor-failure for all $i \in \{1, \dots, 6\}$ satisfies conditions (i), (ii) in Definition 4. We now show the full robustness of the 2Y hexarotor.

Theorem 11. The 2Y hexarotor with $|\alpha - \beta| \in (0, \pi/3]$ is fully robust.

Proof. Fact 10 implies that all the EERs composed of any five rotors of the Yaw-Twisted hexarotor with $|\alpha - \beta| \in (0, \pi/3]$ include the CoM. The 2Y hexarotor is obtained by translating all the P rotors and the N rotors by l and $-l$ along the x-axis of Σ_c from the Yaw-Twisted hexarotor, respectively. Applying Lemma 6, we find that all the EERs composed of any five rotors of the 2Y hexarotor also include the CoM since each EER shape is the same as that of the Yaw-Twisted hexarotor. From Fact 5, the 2Y hexarotor with $|\alpha - \beta| \in (0, \pi/3]$ has an equilibrium such that each element of u_{ss} is greater than zero. We obtain that the 2Y hexarotor with one rotor-failure is (A, B_p) controllable by confirming (6). Therefore, the 2Y hexarotor with $|\alpha - \beta| \in (0, \pi/3]$ is fully robust.

From the geometric hoverability analysis, we find that the Yaw-Twisted hexarotor and the 2Y hexarotor with the same α, β have the same EER. Figure 5 shows the EER of the 2Y hexarotor with $(r, l, \alpha, \beta) = (0.09\ \text{m}, 0.15\ \text{m}, \pi/6, 0)$ in the case of the i-th rotor-failure for all $i \in \{1, \dots, 6\}$. In all the cases, the CoM is included in the EER.

3.3 Optimization of Twisted Angles

The 2Y hexarotor has four design parameters: $r > 0$; $l > 0$; and $\alpha, \beta \in (-\pi/3, \pi/3]$. The hoverability margin is in proportion to r, and independent of l. In this section, we show the relationship between the twisted angles and the hoverability margin, and provide the optimal twisted

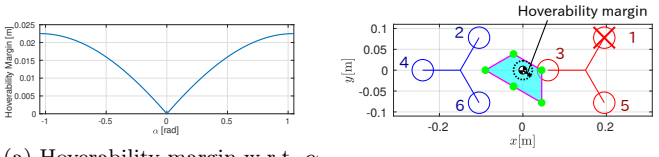

(a) Hoverability margin w.r.t. α

(b) EER at $\alpha = \pi/3$

Fig. 6. Relationship between hoverability margin and α: The calculation is conducted under $(r, l, \beta) = (0.09\ \text{m}, 0.15\ \text{m}, 0)$. (b) shows the EER of the 2Y hexarotor with the 1st rotor-failure at $\alpha = \pi/3$.

angles for the hoverability margin in one rotor-failure case. Here, we fix $(r, l, \beta) = (0.09\ \text{m}, 0.15\ \text{m}, 0)$ and calculate the hoverability margin w.r.t. $\alpha \in (-\pi/3, \pi/3]$ for simple discussion. In the case of a structure with $\beta \neq 0$, we can obtain a structure with the same hoverable region to the structure so that $\beta = 0$ by taking the value of α appropriately. Therefore, the assumption $\beta = 0$ does not lose the generality to investigate the optimal angles.

The hoverability margin of the 2Y hexarotor with one rotor-failure is shown in Fig. 6(a). We find that the hoverablity margin is the largest at $\alpha = \pi/3$. The hoverability margin is zero at $\alpha = 0$ since the CoM is located on the boundary of the EER. In this case, the thrust force of 4th rotor is always zero at an equilibrium, and the system is not (A, B_p) controllable. Thus, the 2Y hexarotor with the 1st rotor-failure is not hoverable at $\alpha = 0$. Fig. 6(b) shows the EER of the 2Y hexarotor with the 1st rotor-failure at $\alpha = \pi/3$. The CoM is included in the interior of the EER. In the case of another rotor-failure, the EER is obtained as the congruent shape, i.e., the same shape or the rotated shape. Therefore, the hoverability margin is always greater than zero even if an arbitrary rotor is failed. Consequently, we obtain that $(\alpha, \beta) = (\pi/3, 0)$ is the optimal solution in the sense of the margin for the full robustness.

Generally, twisted angles such that $|\alpha - \beta| = \pi/3$ are the optimal angles for the 2Y hexarotor. The same statement holds in the case of the Yaw-Twisted hexarotor, which means the Y-shaped hexarotor is the optimal structure. However, the Y-shaped hexarotor has the overlap of two rotors, which causes the degradation of the rotor thrust force. The proposed 2Y hexarotor avoids the degradation by adjusting the value of l while keeping the EER.

4. DESIGN OPTIMIZATION FOR MANEUVERABILITY AND HOVERABILITY

In this section, we provide a design scheme for a hexarotor UAV to maximize its manipulability while ensuring the full robustness for both task performance and safety. Then, the application example for the 2Y hexarotor is presented.

4.1 Optimization Method

We assume that the translational and angular velocity are zeros at the initial state of the vehicle. The translational and angular acceleration of the vehicle is described by

$$\begin{bmatrix} \dot{v} \\ \dot{\omega} \end{bmatrix} = \begin{bmatrix} mI_3 & O_{3\times3} \\ O_{3\times3} & J \end{bmatrix}^{-1} \begin{bmatrix} O_{2\times6} \\ 1 \quad \cdots \quad 1 \\ C_\tau \end{bmatrix} u + \begin{bmatrix} O_{2\times1} \\ g \\ O_{3\times1} \end{bmatrix}. \quad (7)$$

Note that the translational acceleration is independent of the structure. Then, we only consider the rotational dynamics of the vehicle. From (7), the DMM of a hexarotor UAV is obtained as follows based on Yoshikawa (1985):

$$w_d = \sqrt{\det(J^{-1} C_\tau C_\tau^T (J^{-1})^T)} \geq 0.$$

The DMM w_d evaluates the input-output relationship between the rotor thrust forces and angular acceleration. A hexarotor UAV with large w_d can generate the large angular acceleration with small rotor thrust forces. The maximization of w_d implies the maximization of the manipulability of a hexarotor UAV.

We add the following two constraints for safety and efficiency of thrust forces to the maximization problem of w_d.

Full robustness margin: We require the hoverability margin with one rotor-failure $H \in \mathbb{R}$ to be larger than a constant $S > 0$:

$$H \geq S. \quad (8)$$

The constant S is decided based on a safety requirement of a task which the hexarotor conducts. It is difficult to calculate the hoverablity margin analytically for a general structure. However, we can obtain the analytical form for the 2Y hexarotor with $|\alpha - \beta| = \pi/3$ as $H = r/4$.

Non-overlap between two rotors: Each rotor should be placed without any overlap to reduce the degradation of rotor thrust forces. This constraint is written by

$$\sqrt{(x_i - x_j)^2 + (y_i - y_j)^2} \geq D_p + \varepsilon, \quad i < j,\ i, j \in \{1, \ldots, 6\}, \quad (9)$$

where $D_p > 0$ is the diameter of each rotor, and $\varepsilon > 0$ is the small constant as a margin. The diameter of rotors does not directly affect the hoverability analysis. However, we need to make the diameter large enough for the rotor to be able to generate larger thrust force than each element of u_{ss}. This makes it difficult for the Yaw-Twsited hexarotor to avoid having an overlap of two rotors, and thus we need to add the translation of P rotors and N rotors.

Then, the optimization problem is described as follows:

$$\text{maximize} \quad w_d \qquad \text{subject to} \quad (8), (9). \quad (10)$$

4.2 Optimization Example

We now show the optimization (10) in the case of the 2Y hexarotor. Let $(\alpha, \beta) = (\gamma, \gamma - \pi/3)$ with $\gamma \in (0, \pi/3]$. Since (α, β) satisfies $|\alpha - \beta| = \pi/3$, the structure is optimal in the sense of the margin for the full robustness as shown in Section 3.3. For the 2Y hexarotor, C_τ is specified from (5) and J is calculated by assuming that the 2Y hexarotor is composed of some parts as follows: the base body; the six rotors; the six rotor arms with length r; and the two frames with length l between the base body and the center of the rotor arms. Then, we design the three parameters: $r > 0$, $l > 0$, $\gamma \in (0, \pi/3]$.

We solve two optimization problems. One is the optimization (10) without (8), and the other is that with (8). Here, we set the parameters as follows: $S = 0.05$ [m], $D_p = 0.152$ [m], and $\varepsilon = 0.01$ [m]. Note that the DMM w_d tends to be larger as r and l become smaller in the feasible solution set under these parameters. The optimization problems are solved by the "fmincon" function from

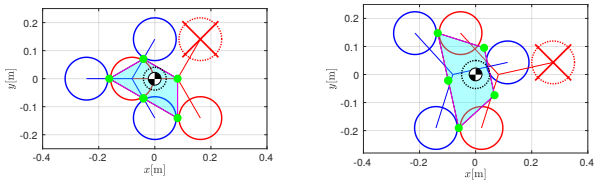

(a) Without constraint (b) With constraint

Fig. 7. Optimization results (a) without the constraint on the full robustness, and (b) with the constraint on the full robustness. The diameter of each red (blue) circle indicates the diameter of each rotor.

the Matlab Optimization Toolbox (MathWorks (2019a)) and the "GlobalSearch" function from the Matlab Global Optimization Toolbox (MathWorks (2019b)).

The result of the optimization without (8) is $(r, l, \gamma) = (0.1624\ \text{m}, 0.0812\ \text{m}, 1.0472\ \text{rad})$. The structure is illustrated in Fig. 7(a). Each parameter is chosen by making r, l smaller to maximize w_d under the constraints for non-overlap. We can find that $\gamma = \pi/3$ is suitable to maximize w_d without the full robustness margin constraint. On the other hand, the result of the optimization with (8) is $(r, l, \gamma) = (0.200\ \text{m}, 0.0812\ \text{m}, 0.2175\ \text{rad})$. The structure is shown in Fig. 7(b). Each parameter is chosen to maximize w_d while satisfying the constraint on the margin for the full robustness. Under the full robustness margin constraint, r should be greater than or equal to $4S$. However, the optimization cannot make r larger than $4S$ with small l at $\gamma = \pi/3$ due to the non-overlap constraint. As a result, the optimization makes r larger and not to change l by varying γ, which does not affect w_d.

The design scheme provides the optimal solution in the sense of the manipulability of the vehicle while ensuring the requirement of safety performance.

5. CONCLUSION

In this paper, we proposed the novel structure of hexarotor UAVs, called 2Y hexarotor. The structure is fully robust against a rotor-failure and reduces the degradation of the thrust force. For this structure, our contributions are as follows: (i) the full robustness is proved using the geometric hoverability analysis; (ii) the optimal twisted angles in the sense of the full robustness are presented by evaluating the hoverability margin; and (iii) the design scheme for the physical parameters of the UAV is proposed based on the DMM and the hoverability margin. Finally, we showed the example of design optimization.

For future work, we will perform the experimental validation of the 2Y hexarotor and consider fault tolerant control in a task such as transportation. The experimental investigations will clarify differences between the standard hexarotor and the 2Y hexarotor in practical applications.

REFERENCES

Anzai, T., Zhao, M., Nozawa, S., Shi, F., Okada, K., and Inaba, M. (2018). Aerial grasping based on shape adaptive transformation by halo: Horizontal plane transformable aerial robot with closed-loop multilinks structure. *2018 IEEE International Conference on Robotics and Automation (ICRA)*, 6990–6996.

Bouabdallah, S., Noth, A., and Siegwart, R. (2004). Pid vs lq control techniques applied to an indoor micro quadrotor. *2004 IEEE/RSJ International Conference on Intelligent Robots and Systems (IROS)*, 3, 2451–2456.

Giribet, J., Sanchez-Pena, R., and Ghersin, A. (2016). Analysis and design of a tilted rotor hexacopter for fault tolerance. *IEEE Transactions on aerospace and electronic systems*, 52(4), 1555–1567.

Kamel, M., Alexis, K., Achtelik, M., and Siegwart, R. (2015). Fast nonlinear model predictive control for multicopter attitude tracking on so(3). 1160–1166.

Kim, S., Choi, S., and Kim, H. (2013). Aerial manipulation using a quadrotor with a two dof robotic arm. 4990–4995.

Kirsch, B., Alexopoulos, A., and Badreddin, E. (2016). Non-linear model based control and parameter identification of a hex-rotor uav. *2016 IEEE International Conference on Systems, Man, and Cybernetics (SMC)*, 002609–002614.

Liang, X., Fang, Y., Sun, N., and Lin, H. (2017). Nonlinear hierarchical control for unmanned quadrotor transportation systems. *IEEE Transactions on Industrial Electronics*, 65(4), 3395–3405.

MathWorks (2019a). fmincon. URL `https://www.mathworks.com/help/optim/ug/fmincon.html`. Last visited on 24/10/2019.

MathWorks (2019b). Globalsearch. URL `https://www.mathworks.com/help/gads/globalsearch.html`. Last visited on 24/10/2019.

Matsuda, R., Ibuki, T., and Sampei, M. (2018). A hoverability analysis method for multirotor uavs with a case study on fault tolerance. In *57th IEEE Conference on Decision and Control (CDC)*, 4264–4269. IEEE.

Michieletto, G., Markus, R., and Franchi, A. (2018). Fundamental actuation properties of multirotors: Force–moment decoupling and fail–safe robustness. *IEEE Transactions on Robotics*, 34(3), 702–715.

Otsuka, H. and Nagatani, K. (2016). Thrust loss saving design of overlapping rotor arrangement on small multirotor unmanned aerial vehicles. 3242–3248.

Schneider, T., Ducard, G., Rudin, K., and Strupler, P. (2012). Fault-tolerant control allocation for multirotor helicopters using parametric programming. *International Micro Air Vehicle Conference and Flight Competition (IMAV)*.

Tadokoro, Y., Ibuki, T., and Sampei, M. (2017). Maneuverability analysis of a fully-actuated hexrotor uav considering tilt angles and arrangement of rotors. *IFAC-PapersOnLine*, 50(1), 8981–8986.

Tayebi, A. and McGilvray, S. (2006). Attitude stabilization of a vtol quadrotor aircraft. *IEEE Transactions on control systems technology*, 14(3), 562–571.

Vazquez-Nicolas, J., Zamora, E., Gonzalez-Hernandez, I., Lozano, R., and Sossa, H. (2018). Towards automatic inspection: crack recognition based on quadrotor uav-taken images. 654–659.

Vey, D. and Lunze, J. (2015). Structural reconfigurability analysis of multirotor uavs after actuator failures. 5097–5104.

Yoshikawa, T. (1985). Manipulability of robotic mechanisms. *The international journal of Robotics Research*, 4(2), 3–9.